Homochiral Metal−Organic Frameworks Based on Transition Metal Bisphosphonates

Owen R. Evans, David R. Manke, and Wenbin Lin*

Department of Chemistry, CB#3290, University of North Carolina, Chapel Hill, North Carolina 27599

Received March 14, 2002. Revised Manuscript Received May 20, 2002

Homochiral metal−organic frameworks with binaphthylbisphosphonate bridging ligands [Mn(**L**-H_2)(MeOH)]·(MeOH), **1**, [Co_2(**L**-H_2)$_2$(H_2O)$_3$]·(H_2O)$_4$, **2**, [Ni(**L**-H_2)($MeOH$)$_4$], **3**, [Cu(**L**-Et_2)], **4**, and [Zn_3(**L**-H)$_2$(C_6H_5N)$_2$], **5**, where **L** is completely deprotonated enantiopure 2,2′-diethoxy-1,1′-binaphthalene-6,6′-bisphosphonic acid, were synthesized under hydro(solvo)-thermal reactions. Single-crystal X-ray diffraction studies reveal that **3**−**5** adopt condensed network structures, while compounds **1** and **2** adopt robust three-dimensional open-framework structures possessing rhombohedral channels. Solid-state circular dichroism spectra indicate that compounds **1**−**5** made from bridging ligands of opposite handness are supramolecular enantiomers. Compounds **1**, **5**, and **L**-H_4 exhibit strong blue fluorescence in solid state, and the formation of excimers in **5** and **L**-H_4 in solid state correlates well with the $\pi-\pi$ stacking interactions. The present work illustrates the potential of rational synthesis of robust chiral porous network solids. The chiral pockets and functionalities within crystalline chiral porous solids may find important applications in enantioselective processes.

Introduction

The recent surge of interest in the field of solid-state supramolecular chemistry has been motivated by the prospect of predictably synthesizing materials with desired chemical and physical properties. Judicious combinations of a vast array of organic ligands and diverse metal coordination geometries can lead to novel metal−organic frameworks that can be potentially exploited for a wide range of important applications such as second-order nonlinear optics, molecule-based magnetism, molecular adsorption,[1] ion exchange,[2] and catalysis.[3] Although the past few years have witnessed significant advances in the synthesis of polymeric metal−organic frameworks with diverse structures,[1−7] there are far fewer reports on the design of functional coordination networks. Motivated by our recent success in the crystal engineering of polar metal−organic coordination networks for second-order nonlinear optical (NLO) applications,[5] we have recently become interested in the rational design of chiral porous metal−organic networks using enantiopure starting materials.

In contrast to traditional inorganic zeolites, which are typically synthesized under harsh conditions and are thus not amenable to the fine-tuning of subtle features such as chemical functionality and chirality, metal−organic frameworks are synthesized under mild conditions and allow systematic engineering of desired chemical and physical properties via modifications of their constituent building blocks. Specifically, the incorporation of chiral bridging ligands into the metal−organic frameworks will necessarily result in chiral solids that can possess chiral pockets or functionalities within the open channels or cavities. Such chiral porous solids hold promise in applications such as enantioselective separation and asymmetric catalysis.[4a,6] We report in this paper the synthesis and characterization of five novel homochiral transition metal bisphosphonates based on enantiopure 2,2′-diethoxy-1,1′-binaphthalene-6,6′-bisphosphonic acid.

Results and Discussion

Synthesis of 2,2′-Diethoxy-1,1′-binaphthalene-6,6′-bisphosphonic Acid, (L-H_4). Compound **L**-H_4 was synthesized in 65% overall yield in four steps starting from the commercially available enantiopure 1,1′-bi-2-naphthol (Scheme 1). Bromination of 1,1′-bi-2-naphthol

* Corresponding author. Fax: (919) 962-2388. E-mail: wlin@unc.edu.

(1) (a) Noro, S.-I.; Kitagawa, S.; Kondo, M.; Seki, K. *Angew. Chem.* **2000**, *112*, 2161−2164; *Angew. Chem., Int. Ed.* **2000**, *39*, 2082−2084. (b) Chen, B.; Eddaoudi, M.; Hyde, S. T.; O'Keeffe, M.; Yaghi, O. M. *Science* **2001**, *291*, 1021−1023. (c) Kondo, M.; Shimamura, M.; Noro, S.-I.; Minakoshi, S.; Asami, A.; Seki, K.; Kitagawa, S. *Chem. Mater.* **2000**, *12*, 1288−1299.

(2) Lee, E.; Kim, J.; Heo, J.; Whang, D.; Kim, K. *Angew. Chem., Int. Ed.* **2001**, *40*, 399−402.

(3) Fujita, M.; Kwon, Y. J.; Washizu, S.; Ogura, K. *J. Am. Chem. Soc.* **1994**, *116*, 1151−1152.

(4) (a) Seo, J. S.; Whang, D.; Lee, H.; Jun, S. I.; Oh, J.; Jeon, Y. J.; Kim, K. *Nature* **2000**, *404*, 982−986. (b) Kiang, Y.-H.; Gardner, G. B.; Lee, S.; Xu, Z.; Lobkovsky, E. B. *J. Am. Chem. Soc.* **1999**, *121*, 8204−8215.

(5) (a) Lin, W.; Evans, O. R.; Xiong, R.-G.; Wang, Z. *J. Am. Chem. Soc.* **1998**, *120*, 13272−13273. (b) Lin, W.; Wang, Z.; Ma, L. *J. Am. Chem. Soc.* **1999**, *121*, 11249−11250. (c) Evans, O. R.; Xiong, R.-G.; Wang, Z.; Wong, G. K.; Lin, W. *Angew. Chem., Int. Ed.* **1999**, *38*, 536−538. (d) Lin, W.; Ma, L.; Evans, O. R. *Chem. Commun.* **2000**, 2263−2264. (e) Evans, O. R.; Lin, W. *Chem. Mater.* **2001**, *13*, 2705−2712.

(6) (a) Evans, O. R.; Ngo, H. L.; Lin, W. *J. Am. Chem. Soc.* **2001**, *123*, 10395−10396. (b) Cui, Y.; Evans, O. R.; Ngo, H. L.; White, P. S.; Lin, W. *Angew. Chem., Int. Ed.* **2002**, *41*, 1159.

(7) (a) Yaghi, O. M.; Li, H.; Davis, C.; Richardson, D.; Groy, T. L. *Acc. Chem. Res.* **1998**, *31*, 575−585. (b) Janiak, C. *Angew. Chem., Int. Ed.* **1997**, *36*, 1431−1434. (c) Chui, S. S.-Y.; Lo, S. M.-F.; Charmant, J. P. H.; Orpen, A. G.; Williams, I. D.; Kepert, C. J.; Prior, T. J.; Rosseinsky, M. J. *J. Am. Chem. Soc.* **2000**, *122*, 5158−5168.

10.1021/cm0202714 CCC: $22.00
Published on Web 08/08/2002

Scheme 1. Synthesis of Ligand L-H_4

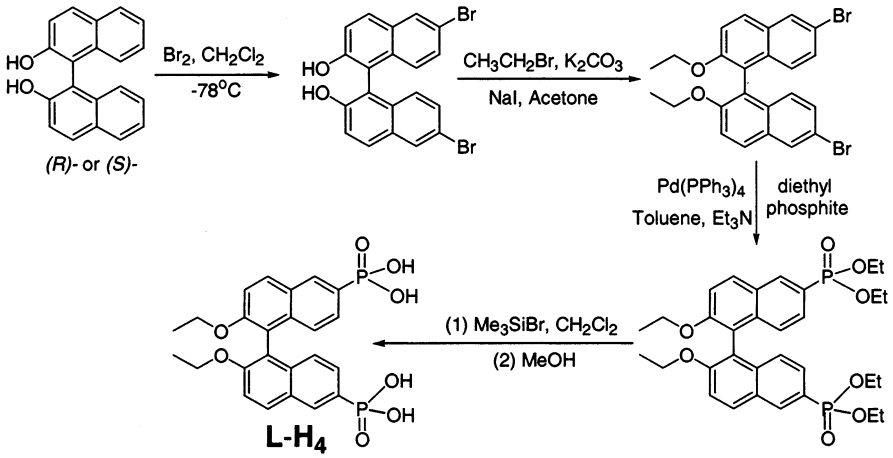

Scheme 2. Synthesis of Compounds 1−5

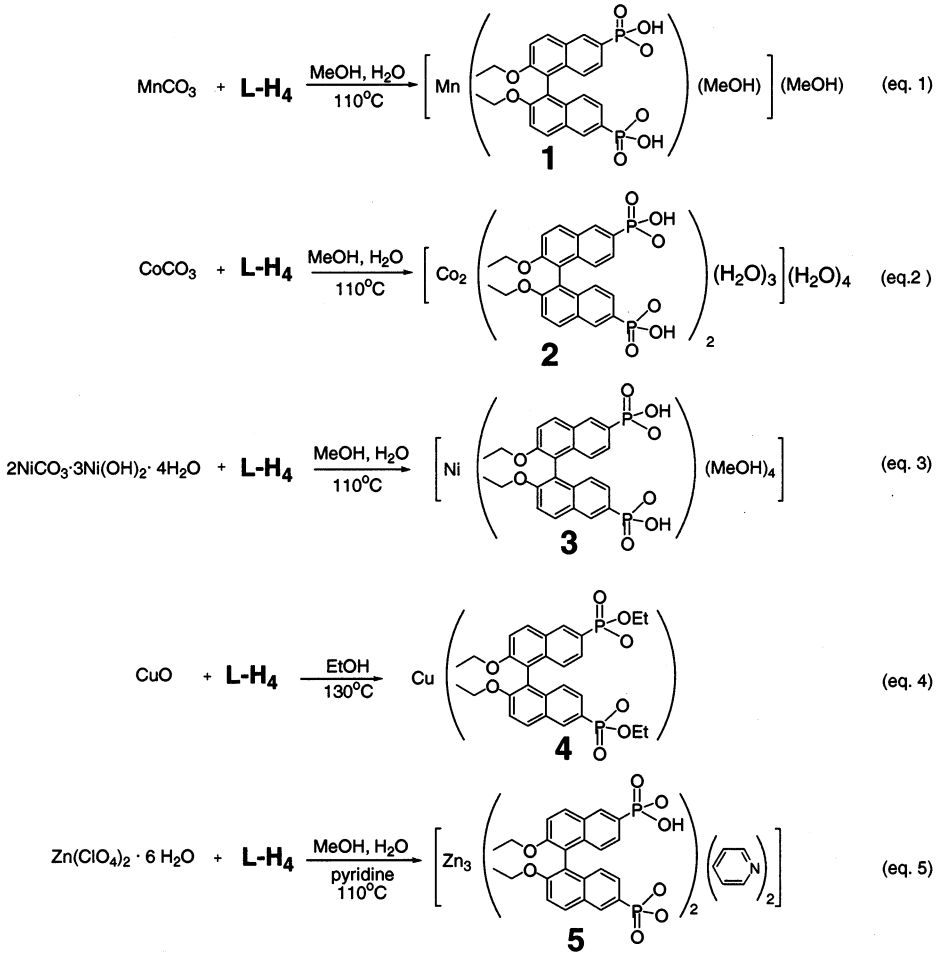

at −78 °C afforded 6,6′-dibromo-2,2′-dihydroxy-1,1′-binaphthalene in nearly quantitative yield.[1] Protection of the 2,2′-hydroxy groups with bromoethane afforded pure 6,6′-dibromo-2,2′-diethoxy-1,1′-binaphthalene in quantitative yield.[8] A palladium-catalyzed phosphonation reaction with diethyl phosphite, using $Pd(PPh_3)_4$ as catalyst, then afforded tetraethyl-2,2′-diethoxy-1,1′-binaphthalene-6,6′-diphosphonate in 67% isolated yield.[2] Treatment of this tetraethyl bisphosphonate with trimethylsilyl bromide followed by hydrolysis with methanol afforded **L**-H_4 in quantitative yield.[3] All intermediates and final products were characterized by ^1H $\{^{31}P\}$ NMR, ^{13}C $\{^1H\}$ NMR, and ^{31}P NMR spectroscopies.

Synthesis of Transition Metal Bisphosphonates. [Mn(**L**-H_2)(MeOH)]·(MeOH), **1**, was obtained by a hydro-(solvo)thermal reaction between $MnCO_3$ and 2,2′-diethoxy-1,1′-binaphthalene-6,6′-bisphosphonic acid, **L**-H_4, in a mixture of methanol and water at 110 °C (Scheme 2, eq 1). The infrared spectrum of **1** displays a series of sharp peaks from 922 to 1142 cm^{-1} due to P−O stretches.[4] The IR spectrum of **1** also shows the presence of a broad peak at 3400 cm^{-1} that is due to O−H stretches from coordinated and free methanol molecules. Thermogravimetric (TGA) analysis of **1** revealed a

weight loss of 9.7% by 180 °C, corresponding to the loss of one free methanol and one coordinated methanol per formula unit (calculated 10.3%).

$[Co_2(\mathbf{L}\text{-}H_2)_2(H_2O)_3]\cdot(H_2O)_4$, **2**, was obtained in 78% yield by a hydro(solvo)thermal reaction between $CoCO_3$ and **L**-H_4 in a mixture of methanol and water at 110 °C (Scheme 2, eq 2). The IR spectrum of compound **2** exhibits strong peaks from 939 to 1144 cm^{-1}, attributed to P−O stretches.[11] The IR spectrum of **2** also exhibits a broad peak at ∼3400 cm^{-1} corresponding to the hydroxyl stretch of H_2O. Thermogravimetric analysis of **2** reveals a weight loss of 9.3% by 250 °C, corresponding to the loss of 3 mol of coordinated H_2O and 4 mol of free H_2O per formula unit (calculated 10.1%).

$[Ni(\mathbf{L}\text{-}H_2)(MeOH)_4]$, **3**, was obtained in 82.3% yield via a hydro(solvo)thermal reaction between $2NiCO_3\cdot3Ni(OH)_2\cdot4H_2O$ and **L**-H_4 in methanol at 110 °C (Scheme 2, eq 3). The IR spectrum of **3** displays strong phosphorus−oxygen stretches at 920−1150 cm^{-1}.[11] TGA analyses show that **3** exhibits a weight loss of 18.6% by 145 °C corresponding to the loss of the four coordinated methanol molecules (expected 18.7%).

$[Cu(\mathbf{L}\text{-}Et_2)]$, **4**, was obtained by a hydro(solvo)thermal reaction between CuO and **L**-H_4 in absolute ethanol at 130 °C (Scheme 2, eq 4). The IR spectrum of **4** exhibits strong and sharp peaks from 960 to 1112 cm^{-1}, attributed to the P−O stretches of **L**-Et_2.[11] Interestingly, elemental analysis and single-crystal X-ray diffraction (vide infra) on compound **4** indicate the occurrence of an in situ esterification reaction resulting in the formation of **L**-Et_2. Similar reactions performed in methanol or in the presence of H_2O resulted in unidentified alternate phases or recovered starting materials. Optimal esterification conditions, such as elevated temperatures and anhydrous solvents, were thus found to be essential in the synthesis of **4**.

$[Zn_3(\mathbf{L}\text{-}H)_2(C_6H_5N)_2]$, **5**, was obtained in 86.5% yield from a hydro(solvo)thermal reaction between $Zn(ClO_4)_2\cdot6H_2O$ and **L**-H_4 in a mixture of methanol, water, and pyridine at 110 °C (Scheme 2, eq 5). The IR spectrum of **5** also shows strong P−O stretches at 920−1120 cm^{-1}.[11] TGA analysis of **5** reveals a gradual 9.6% weight loss by 350 °C, corresponding to the loss of 1 mol of pyridine per formula unit (calculated 11.7%). Compounds **1**−**5** are insoluble in common organic solvents, and their formulations have been confirmed by single-crystal X-ray determinations.

X-ray Structure of [Mn(L-H_2)(MeOH)]·(MeOH), 1. A single-crystal X-ray diffraction study on (*R*)-**1** reveals the formation of a complex three-dimensional (3-D) framework consisting of 5-coordinate manganese centers and bridging binaphthylbisphosphonate groups. Compound **1** crystallizes in the chiral space group $P2_12_12_1$. The asymmetric unit consists of one manganese center, one bridging **L**-H_2 group, one coordinated methanol molecule, and one methanol guest molecule (Figure 1a). The Mn center adopts a distorted trigonal bipyramidal geometry by coordinating to one methanol molecule and to four oxygen atoms of four different **L**-H_2 groups. The O−Mn−O angles deviate slightly from the ideal trigonal bipyramidal geometry, with the angles lying in the trigonal plane ranging from 101.5(2)° to 137.8(2)° and the trans O3−Mn−O1b angle measuring 172.3(2)°. The two naphthyl rings of the bridging **L**-H_2 group have a dihedral angle of 115.49°. A closer examination of the crystal structure of **1** reveals that monodeprotonated **L**-H_2 groups coordinate to adjacent Mn centers via a μ_2,η^2-phosphonato bridge, resulting in the formation of infinite $[Mn(PO_3H)_2]_\infty$ chains running along the *a*-axis (Figure 1b). Adjacent phosphonato bridges along the chain are approximately offset 90° from one another. Bridging **L**-H_2 groups thus connect every $[Mn(PO_3H)_2]_\infty$ chain to four adjacent chains to result in a 3-D framework with rhombohedral channels. These channels run along the *a*-axis and have an approximate size of 5.3 × 2.7 Å (Figure 2). The limited void space in **1** is thus effectively filled via the inclusion of one methanol guest per formula unit.

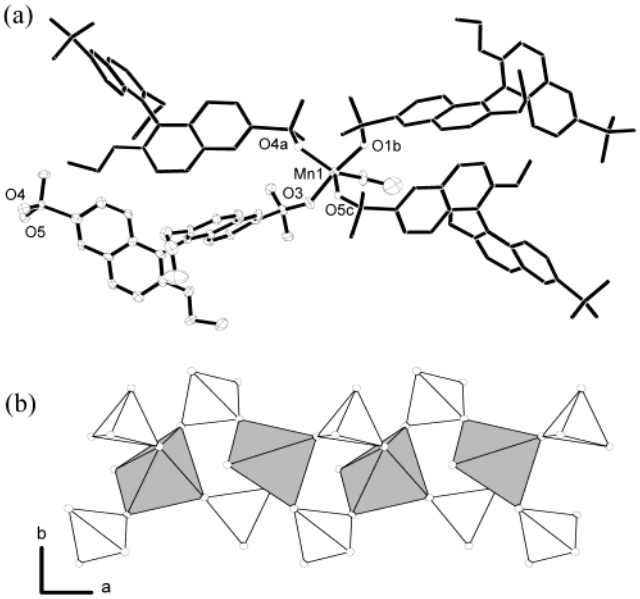

Figure 1. (a) Coordination environment of **1**. Asymmetric unit shown as ellipsoids at 60% probability. (b) View of the infinite $[Mn(PO_3H)_2]$ chains along the *c*-axis. The coordination environments of Mn and P atoms are represented by gray and white polyhedra, respectively.

X-ray Structure of $[Co_2(\mathbf{L}\text{-}H_2)_2(H_2O)_3]\cdot(H_2O)_4$, 2. A single-crystal X-ray diffraction study of (*R*)-**2** revealed the formation of a complex 3-D metal−organic framework containing bridging **L**-H_2 groups and both 6- and 4-coordinate Co(II) centers. Compound **2** crystallizes in the chiral space group $P2_1$. The asymmetric unit consists of two Co(II) centers, two bridging **L**-H_2 groups, three coordinated H_2O molecules, and four H_2O guest molecules (Figure 3). The two Co(II) centers adopt drastically different coordination geometries. The Co1 center adopts a distorted octahedral geometry by coordinating in a fac configuration to three oxygens atoms of three different **L**-H_2 groups and to three oxygen atoms of three coordinated H_2O molecules. The cis O−Co1−O angles range from 83.99(1)° to 98.41(1)° while trans O−Co1−O angles range from 168.3(1)° to 173.88(1)°. The Co2 center, on the other hand, adopts a tetrahedral geometry

(8) Duessen, H. J.; Hendrickx, E.; Boutton, C.; Krog, D.; Clays, K.; Bechgaard, K.; Persoons, A.; Bjornholm, T. *J. Am. Chem. Soc.* **1996**, *118*, 6841−6852.
(9) Hirao, T.; Masunaga, T.; Yamada, N.; Ohshiro, Y.; Agawa, T. *Bull. Chem. Soc. Jpn.* **1982**, *55*, 909−913.
(10) Jaffrès, P.-A.; Bar, N.; Villemin, D. *J. Chem. Soc., Perkin Trans. 1* **1998**, 2083−2089.
(11) Corbridge, D. E. C. *Phosphorus: An Outline of its Chemistry, Biochemistry and Technology*, 4th ed.; Elsevier Scientific Publishing Company: New York, 1990.

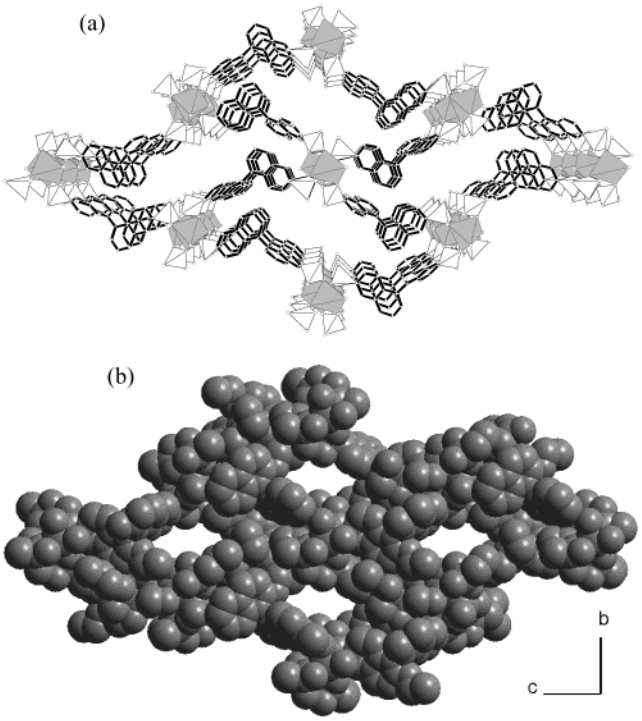

Figure 2. (a) View of the 3-D framework and rhombohedral channels of **1** down the *a*-axis. The coordination environments of Mn and P atoms are represented by gray and white polyhedra, respectively. Methanol guests and 2,2′-ethoxy groups are omitted for clarity. (b) A space-filling model of **1** as viewed down the *a*-axis.

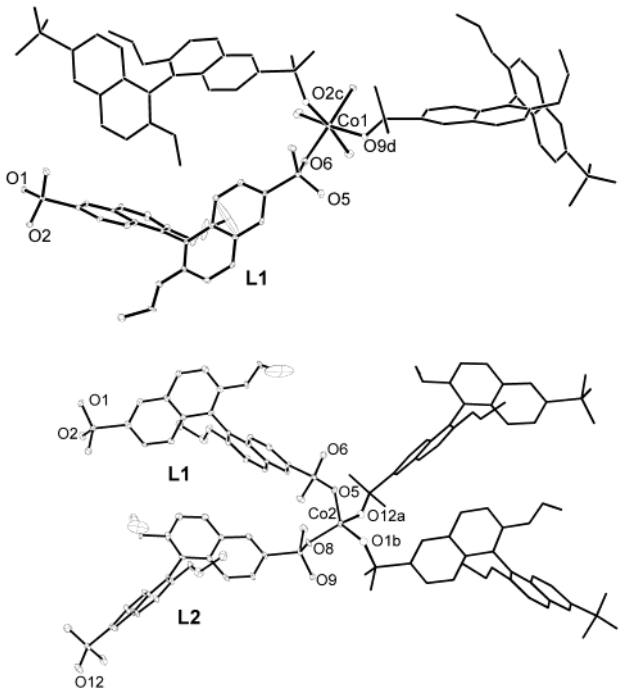

Figure 3. Coordination environment of **2**. Asymmetric unit is shown as ellipsoids at 60% probability. For clarity H_2O guests have been removed. The asymmetric unit has been broken up into two units to clearly show the two different Co(II) environments. Bridging ligand **L1**-H_2 has been duplicated to show the connectivity between the two cobalt centers.

by coordinating to four oxygen atoms of four different **L**-H_2 groups. The O−Co2−O angles deviate slightly from the ideal tetrahedral geometry and range from

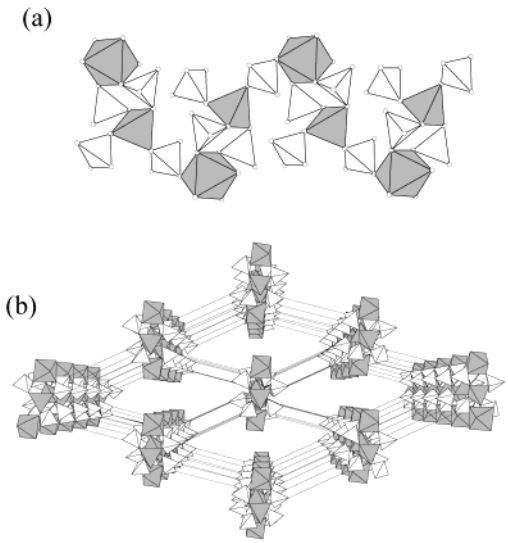

Figure 4. (a) View of the infinite $[Co(H_2O)_3(PO_3H)_2{\cdot}Co(PO_3H)_2]$ chain in **2** along the *c*-axis. The coordination environments of the Co and P atoms are represented as gray and white polyhedra, respectively. (b) View of the 3-D framework of **2** along the *b*-axis. The coordination environments of Co and P atoms are represented as gray and white polyhedra, respectively. The binaphthyl backbones of **L**-H_2 are represented as straight lines.

104.29(1)° to 113.65(1)°. The two binaphthyl subunits of **L1** and **L2** have dihedral angles of 115.52° and 113.75°, respectively. Three phosphonate groups of the two crystallographically unique **L**-H_2 groups coordinate to adjacent metal centers via a μ_2,η^2-phosphonato bridge. Two of these bridges coordinate to the same two cobalt centers to form a dimetal linkage, while the third connects adjacent dimetal units to form infinite $[Co(H_2O)_3(PO_3H)_2{\cdot}Co(PO_3H)_2]_\infty$ helical chains running along the *b*-axis (Figure 4a). The fourth phosphonate group coordinates in a monodentate fashion to the tetrahedral Co2 centers. Similar to **1**, adjacent phosphonate groups along the $[Co(H_2O)_3(PO_3H)_2{\cdot}Co(PO_3H)_2]_\infty$ chains are approximately offset by ∼90°. Bridging **L**-H_2 groups thus connect every $[Co(H_2O)_3(PO_3H)_2{\cdot}Co(PO_3H)_2]_\infty$ chain to four structurally identical chains to result in a 3-D framework containing rhombohedral channels running along the *b*-axis (Figure 4b). These rhombohedral channels are approximately 3.4 × 4 Å in size and are occupied by four H_2O molecules per formula unit.

X-ray Structure of [Ni(L-H_2)(MeOH)$_4$], 3. A single-crystal X-ray diffraction study of (*R*)-**3** reveals the formation of a one-dimensional (1-D) zigzag coordination polymer consisting of 6-coordinate Ni centers and bridging binaphthylbisphosphonate groups. Compound **3** crystallizes in the chiral space group $P2_12_12_1$. The asymmetric unit of **3** consists of one Ni center, one bridging binaphthylbisphosphonate group, and four coordinated methanol molecules (Figure 5a). The Ni center adopts a slightly distorted octahedral geometry by coordinating to four methanol molecules and to two oxygen atoms of two different binaphthylbisphosphonate ligands (trans O−Ni−O angles range from 169.49(1)° to 174.04(1)° and cis O−Ni−O angles range from 84.09(1)° to 97.35(1)°). The two phosphonate groups are monodeprotonated and coordinate to the Ni center in a cis geometry with an O1−Ni−O6A angle of 97.35(1)°. The binaphthyl subunit has a dihedral angle of 115.49°

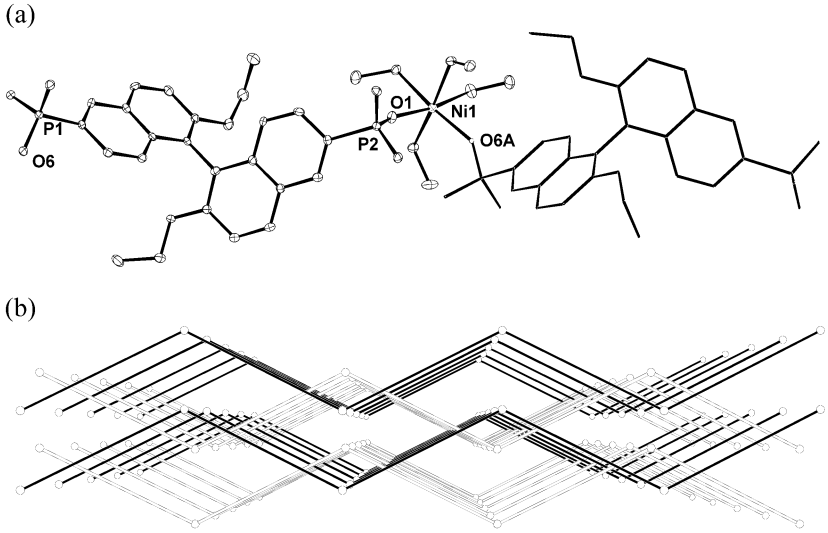

Figure 5. (a) Coordination environment of **3**. Asymmetric unit is shown with ellipsoids at 60% probability. (b) View of the zigzag framework of **3** along the *b*-axis.

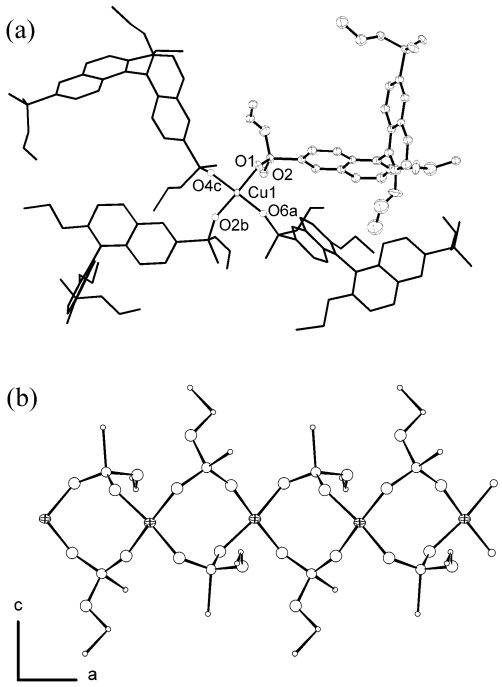

Figure 6. (a) Coordination environment of **4**. Asymmetric unit shown as ellipsoids at 60% probability. (b) View of the infinite $[Cu(PO_3Et)_2]$ chains along the *c*-axis. Cu(II) centers are represented as ellipsoids at 60% probability while circles with increasing sizes represent C, P, and O, respectively.

and bridges adjacent Ni centers to form an infinite 1-D zigzag chain running parallel to the *c*-axis. A close examination of the X-ray structure of **3** reveals that adjacent chains pack in registry along the *a*-axis; however, 2_1 symmetry causes adjacent chains along the *b*-axis to adopt a staggered formation (Figure 5b). The 1-D structure of **3** is further stabilized by hydrogen bonding between phosphonic acid functionalities and coordinated methanol molecules to form a 3-D hydrogen-bonded network (Figure 6). Although we have not been able to locate hydrogen atoms on coordinated methanol molecules and phosphonic acid moieties, the presence of hydrogen bonds in **3** can be readily inferred from the following short oxygen−oxygen contacts: O3···O10, 2.885(5) Å; O2···O11, 2.724(5) Å; O5···O2, 2.417(5) Å;

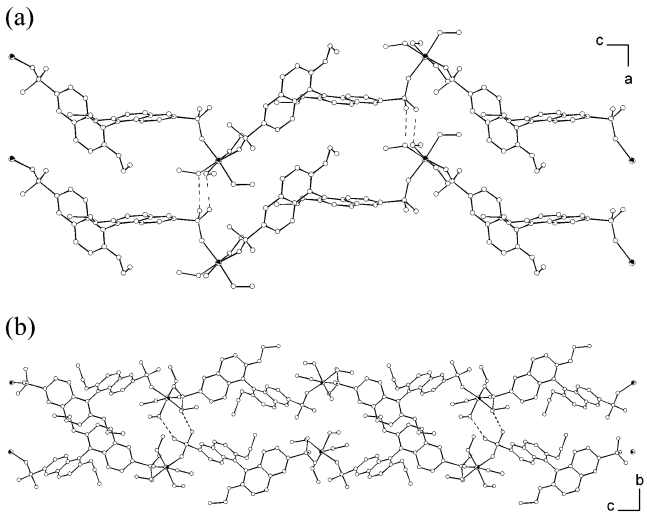

Figure 7. (a) View of **4** along the *b*-axis. (b) View of **4** along the *a*-axis. Hydrogen-bonding interactions are shown as dotted lines.

O4···O9, 2.735(5) Å; O12···O3, 2.677(5) Å; O3···O4, 2.516(5) Å.

X-ray Structure of [Cu(L-Et$_2$)], 4. A single-crystal X-ray diffraction study of (*R*)-**4** revealed the formation of a 3-D metal−organic framework similar in topology to **1**. Compound **4** crystallizes in the chiral space group $P2_12_12_1$. The asymmetric unit consists of one Cu(II) center and one bridging **L**-Et_2 group. The formation of the PO_3Et moiety in **4** results from an in situ esterification reaction between **L**-H_4 and ethanol and is driven by an excess of ethanol and anhydrous conditions. The Cu(II) center adopts a distorted square planar geometry by coordinating to four oxygen atoms of four different **L**-Et_2 groups. The O−Cu−O angles deviate slightly from the ideal square planar geometry (Figure 7a). The cis O−Cu−O angles range from 89.8(2)° to 92.0(3)°, while the trans O1−Cu−O2 and O6−Cu−O4 angles measure 166.1(2)° and 173.2(3)°, respectively. Similar to **1**, the phosphonate groups of **L**-Et_2 coordinate to adjacent Cu(II) centers via a μ_2,η^2-phosphonato bridge, resulting in the formation of $[Cu(PO_3Et)_2]_\infty$ chains running along the *a*-axis (Figure 7b). Every $[Cu(PO_3Et)_2]_\infty$ chain in **4** is connected to four adjacent chains via **L**-Et_2 bridges to

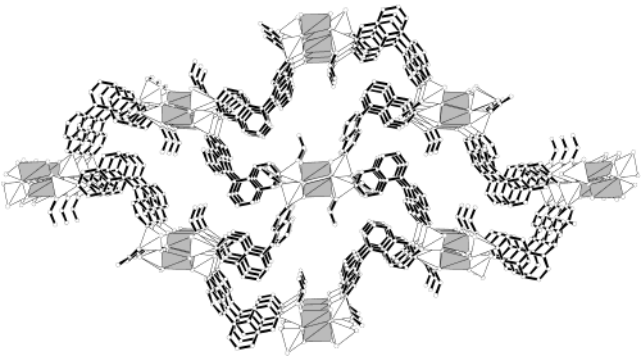

Figure 8. View of the 3-D framework of **4** along the *a*-axis. The coordination environments of Cu and P atoms are represented as gray and white polyhedra, respectively. 2,2′-Ethoxy groups are omitted for clarity.

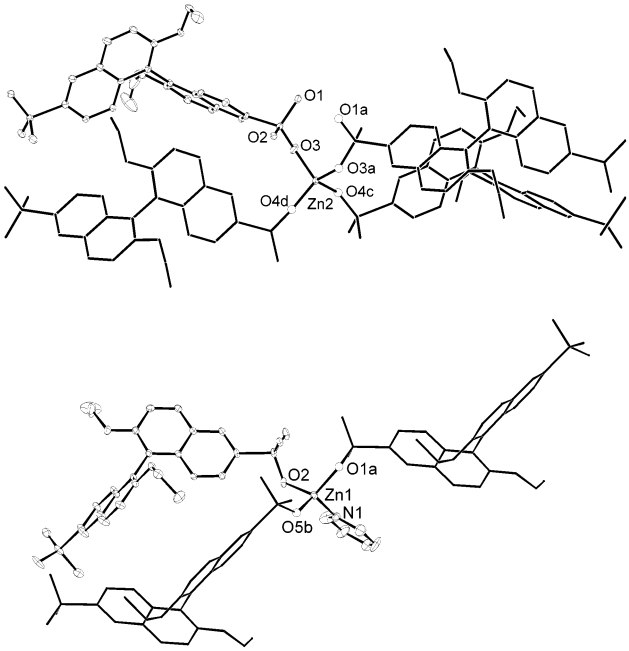

Figure 9. Coordination environments of the Zn centers in **5**. The asymmetric unit is shown as ellipsoids at 50% probability. The bridging **L**-H group has been duplicated to show the connectivity of the Zn centers.

result in a 3-D metal−organic framework with rhombohedral channels running along the *a*-axis (Figure 8). An examination of **4** reveals that the ethyl group of PO_3-Et orients toward the center of these rhombohedral channels. These groups in combination with 2,2′-ethoxy groups effectively fill the void space in these cavities, and as a result, no solvent is enclathrated in compound **4**.

X-ray Structure of $[Zn_3(L\text{-}H)_2(C_6H_5N)_2]$, 5. A single-crystal X-ray diffraction study of **5** revealed the formation of 2-D metal−organic framework consisting of 4-coordinate Zn centers and bridging **L**-H groups. Compound **5** crystallizes in the chiral space group *C*2. The asymmetric unit consists of two Zn centers, one bridging **L**-H group, and one coordinated pyridine. The Zn2 center lies on a crystallographic 2-fold axis and thus has an occupancy of 1/2. The two Zn centers adopt similar coordination geometries (Figure 9). The Zn1 center adopts a distorted tetrahedral geometry by coordinating to one pyridyl nitrogen atom and three oxygen atoms of three different **L**-H groups. The angles

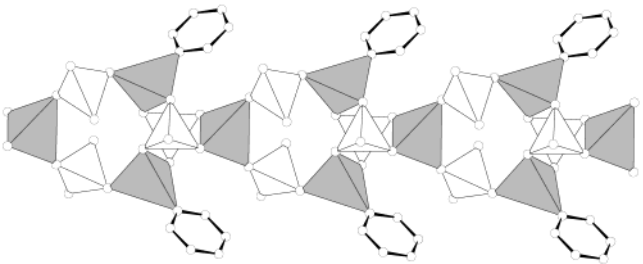

Figure 10. View of the $[Zn(\mu_2,\eta^2\text{-}PO_3H)_2{\cdot}Zn_2(\mu_3,\eta^3\text{-}PO_3)_2(pyr)_2]$ chain in **5**.

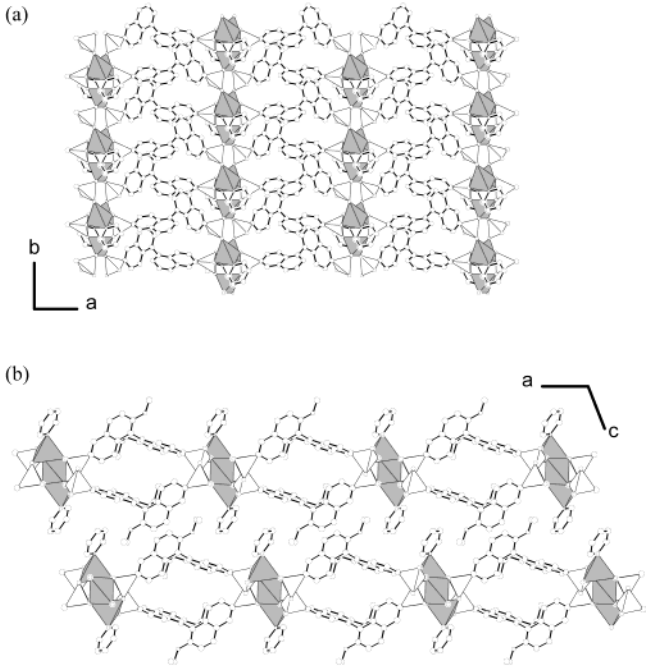

Figure 11. (a) View of the 2-D framework in **5** along the *c*-axis. The 2,2′-ethoxy groups are omitted for clarity. (b) Interdigitation of adjacent 2-D frameworks in **5** as viewed along the *b*-axis.

about the Zn1 center range from 100.04(3)° to 121.42(3)° and deviate slightly from that of an ideal tetrahedron. The Zn2 center adopts a tetrahedral geometry by coordinating to four oxygen atoms of four different **L**-H groups. In contrast to the Zn1 center, the Zn2 center adopts a nearly ideal tetrahedral geometry with O−Zn2−O angles ranging from 102.73(2)° to 115.53(3)°. One of the two crystallographically unique phosphonate groups, P2, is monodeprotonated and links Zn2 centers to two adjacent Zn1 centers via the formation of two μ_2,η^2-phosphonato bridges. The other unique phosphonate group is doubly deprotonated and links a pair of Zn1 centers to an adjacent Zn2 center via the formation of two μ_3,η^3-phosphonato bridges. These phosphonato bridges repeat to form infinite $[Zn(\mu_2,\eta^2\text{-}PO_3H)_2{\cdot}Zn_2(\mu_3,\eta^3\text{-}PO_3)_2(pyr)_2]_8$ chains that run along the *b*-axis (Figure 10).

The binaphthyl backbone of the bridging **L**-H group has a dihedral angle of 113.88°. Each $[Zn(\mu_2,\eta^2\text{-}PO_3H)_2{\cdot}Zn_2(\mu_3,\eta^3\text{-}PO_3)_2(pyr)_2]_\infty$ chain is linked to two adjacent chains via bridging **L**-H groups to form an infinite two-dimensional (2-D) grid lying in the *ab*-plane (Figure 11a). Adjacent 2-D grids interdigitate via the aromatic $\pi-\pi$ stacking of coordinated pyridine molecules along the *a*-axis (Figure 11b). These interdigitated pyridine

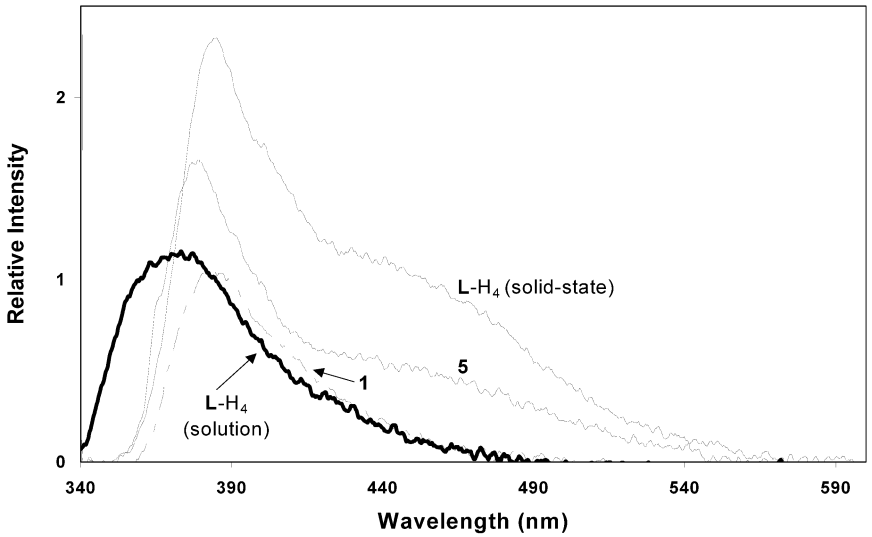

Figure 12. Fluorescent spectra of **1**, **5**, and **L**-H_4 in the solid state at room temperature. The emission spectrum of **L**-H_4 in methanol is also illustrated ($\lambda_{ex} = 338$ nm).

rings have a centroid−centroid distance of 3.988 Å and a shortest contact of 3.036 Å. The interdigitation in **5** has effectively filled any void space, resulting in the formation of a condensed solid with no clathration of solvent molecules.

X-ray Structure of L-H$_4$.[12] **L**-H_4 crystallizes in the chiral space group $P2_1$ and has a dihedral angle of 120.0° between the two naphthyl rings, similar in magnitude to that of compound **3**. The free ligand also adopts an extensive hydrogen-bonded 3-D network. The presence of hydrogen bonds can be inferred from the following short O−O contacts: O2···O1, 2.591 Å; O1···O5, 2.615 Å; O3···O6, 2.578 Å; O6···O4, 2.548 Å.

Photoluminescence and Chiroptical Properties. The UV−vis spectrum of **L**-H_4 in methanol exhibits an intense absorbance at ∼338 nm which can be assigned to an intramolecular $\pi \rightarrow \pi^*$ transition. The luminescent spectra ($\lambda_{ex} = 338$ nm) of **1** and **5** in the solid state at room temperature exhibit intense bands at $\lambda_{max} = 386$ and 380 nm for **1** and **5**, respectively (Figure 12). These emissions can be tentatively ascribed to an intraligand $\pi \rightarrow \pi^*$ transition since a similar emission was also observed for free **L**-H_4 in the solid state. Compounds **5** and **L**-H_4 also exhibit a broad longer wavelength emission consistent with excimer formation. The degree of excimer formation correlates well with the degree of aromatic $\pi-\pi$ interactions observed in the solid state. The shortest centroid−centroid distance between naphthyl rings in **L**-H_4 and **5** are 4.916 and 4.861 Å, and excimer formation has been observed in both **L**-H_4 and **5**. In contrast, **1** adopts an open framework with no aromatic $\pi-\pi$ interactions and thus exhibits no longer wavelength emission that can be attributed to excimer formation.

Solid-state circular dichroism (CD) spectra were obtained from KBr pellets for compounds **1**−**5** from both the (*R*)- and (*S*)-enantiomers of **L**-H_4.[13] The CD spectra of the (*R*)- and (*S*)-isomers of **1**−**5** are identical mirror images, indicating the expected formation of supramolecular enantiomers (Figure 13).

Discussion

The past few years have borne witness to a rapid expansion in the field of metal phosphonate chemistry.[14] These unique materials allow one to design solids with a highly robust yet flexible framework. The organic group of the phosphonate ligand can be chemically modified to allow for the synthesis of materials with desired physical and chemical properties. Notable examples include the use of α,ω-bisphosphonic acids in the synthesis of porous lamellar solids.[15] With a few exceptions,[7,16] the use of enantiopure starting materials in the synthesis of porous metal phosphonates has not been investigated. The present work has outlined the design of novel enantiopure bisphosphonates and has successfully shown their potential in the construction of porous homochiral metal phosphonate coordination networks. We have also demonstrated that large single crystals of these metal phosphonate compounds can be readily obtained by utilizing insoluble metal salts and hydro(solvo)thermal conditions. Despite the elevated temperature of hydro(solvo)thermal synthesis, compounds **1** and **2** have interesting open-framework structures and clearly show the potential of these materials in the design of homochiral porous solids. Further work is aimed at increasing the porosity of these frameworks through alternative crystallization methods and structural modifications of bisphosphonate bridging ligand.

Experimental Section

Materials and Methods. Cobalt(II) carbonate, copper(II) oxide, and manganese(II) carbonate were purchased from

(12) Crystal data for **L**-H_4: monoclinic space group $P2_1$, $a = 12.310(1)$ Å, $b = 7.525(1)$ Å, $c = 13.923(1)$ Å, $\beta = 114.075(1)°$, $V = 1178.2(2)$ Å^3, and $Z = 2$.

(13) Kuroda, R.; Honma, T. *Chirality* **2000**, *12*, 269−277.

(14) (a) Clearfield, A. *Chem. Mater.* **1998**, *10*, 2801−2810. (b) Clearfield, A. *Prog. Inorg. Chem.* **1998**, *47*, 371−510. (c) Mallouk, T. E.; Gavin, J. A. *Acc. Chem. Res.* **1998**, *31*, 209−217.

(15) (a) Byrd, H.; Clearfield, A.; Poojary, D.; Reis, K. P.; Thompson, M. E. *Chem. Mater.* **1996**, *8*, 2239−2246. (b) Alberti, G.; Costantino, U.; Marmottini, F.; Vivani, R.; Zappelli, P. *Angew. Chem., Int. Ed. Engl.* **1993**, *32*, 1357−1359.

(16) Fredoueil, F.; Evain, M.; Bujoli-Doeuff, M.; Bujoli, B. *Eur. J. Inorg. Chem.*, **1999**, *7*, 1077−1079.

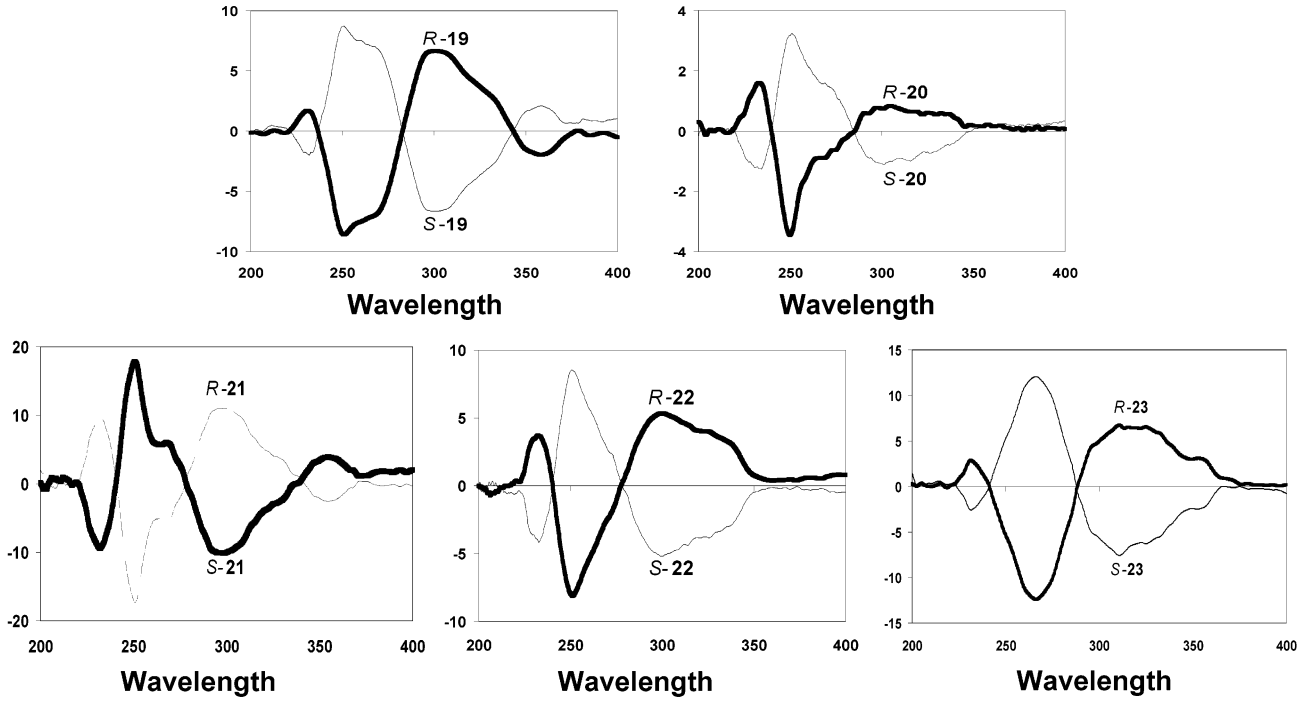

Figure 13. Solid-state circular dichroism spectra of (*R*)- and (*S*)-**1**−**5**.

Table 1. Data for the X-ray Diffraction of 1−5

compound	**1**	**2**	**3**	**4**	**5**
chemical formula	$C_{26}H_{30}MnO_{10}P_2$	$C_{48}H_{58}Co_2O_{23}P_4$	$C_{28}H_{38}NiO_{12}P_2$	$C_{28}H_{30}CuO_8P_2$	$C_{29}H_{26}NO_8P_2Zn_{1.5}$
crystal system	orthorhombic	monoclinic	orthorhombic	orthorhombic	monoclinic
a, Å	7.9137 (7)	14.963 (2)	7.4339 (11)	8.2110 (6)	31.125 (3)
b, Å	12.7304 (11)	12.3428 (17)	13.421 (2)	13.4308 (10)	8.4355 (7)
c, Å	27.357 (2)	16.137 (2)	30.053 (4)	25.664 (2)	11.9507 (10)
β, deg	90	116.589 (3)	90	90	111.521 (2)
V, Å	2756.1 (4)	2665.1 (6)	2998.4 (8)	2830.3 (4)	2918.9 (4)
Z	4	2	4	4	4
formula weight	619.40	1244.73	687.24	620.03	676.56
space group	$P2_12_12_1$	$P2_1$	$P2_12_12_1$	$P2_12_12_1$	C_2
T, °C	−80	−80	−80	−60	−80
λ (Mo Kα), Å	0.710 73	0.710 73	0.710 73	0.710 73	0.710 73
ρ_{calc}, g/cm^3	1.493	1.551	1.522	1.455	1.539
no. unique reflns	4587	11779	7259	6030	5286
no. obsd reflns ($I > 2\sigma(I)$)	2466	4752	4219	4720	3745
N_{params}	415	710	451	212	418
min and max res density, e/Å^3	−0.395, 0.430	−0.730, 0.826	−0.689, 0.521	−0.635, 0.956	−0.744, 0.537
R1	0.046	0.0608	0.0526	0.0800	0.0471
wR2	0.098	0.1251	0.1166	0.2220	0.1177
goodness of fit	0.65	0.813	0.766	1.529	0.795
Flack parameter	−0.05 (4)	0.03 (2)	0.01 (2)	0.06 (3)	0.02 (2)

[a] $R1 = \sum| |F_o| - |F_c| |/\sum|F_o|$; $wR2 = [\sum[w(F_o^2 - F_c^2)^2]/\sum[w(F_o^2)^2]]^{1/2}$; $GOF = [\sum[w(F_o^2 - F_c^2)^2]/(\text{no. of reflections} - \text{no. of parameters})]^{1/2}$.

Aldrich Chemical Co. and used without further purification. Thermogravimetric analysis was performed in air at a scan speed of 10 °C/min on a Shimadzu TGA-50 analyzer. Infrared spectra were measured from KBr pellets on a Perkin-Elmer Paragon 1000 FT-IR spectrometer. Solid-state circular dichroism spectra were measured from KBr pellets on a Jasco-810 spectrometer. Solid-state fluorescence spectra were measured from Nujol mulls on a Shimadzu RF-5301 fluorimeter.

Synthesis of [Mn(L-H$_2$)(MeOH)]·(MeOH), 1. In a heavy-walled Pyrex tube a mixture of $MnCO_3$ (0.022 g, 0.2 mmol) and **L**-H_4 (0.050 g, 0.1 mmol) was thoroughly mixed in methanol (1.0 mL) and H_2O (0.2 mL). The tube was frozen, sealed under vacuum, and placed in an oven at 110 °C. After 24 h of heating, 0.053 g of colorless platelike crystals was obtained (yield: 85.5%, based on **L**-H_4). Anal. Calcd (found) for [Mn(**L**-H_2)(MeOH)]·(MeOH): C, 50.4 (47.8); H, 4.88 (4.17).[17] IR (cm^{-1}): 3406 (br), 1618 (m), 1465 (m), 1340 (w), 1268 (w), 1234 (w), 1142 (s), 1043 (s), 922 (s), 827 (w), 806 (w), 663 (w), 546 (w).

Synthesis of [Co$_2$(L-H$_2$)(H$_2$O)$_3$]·(H$_2$O)$_4$, 2. In a heavy-walled Pyrex tube a mixture of $CoCO_3$ (0.024 g, 0.2 mmol) and **L**-H_4 (0.050 g, 0.1 mmol) was thoroughly mixed in methanol (1.0 mL) and H_2O (0.2 mL). The tube was frozen, sealed under vacuum, and placed in an oven at 110 °C. After 24 h of heating, 0.049 g of blue platelike crystals was obtained (yield: 78.3%, based on **L**-H_4). Anal. Calcd (found) for [Co_2(**L**-H_2)(H_2O)$_3$]·(H_2O)$_4$: C, 46.3 (44.3); H, 4.70 (4.13). IR (cm^{-1}): 3426 (br), 1619 (s), 1485 (w), 1467 (w), 1340 (w), 1277 (m), 1250 (m), 1144 (s), 1112 (s), 1047 (s), 939 (w), 823 (w), 666 (w), 572 (w).

Synthesis of [Ni(L-H$_2$)(MeOH)$_4$], 3. A heavy-walled Pyrex tube containing a mixture of $2NiCO_3 \cdot 3Ni(OH)_2 \cdot 4H_2O$ (0.0150 g, 0.025 mmol) and **L**-H_4 (0.0377 g, 0.075 mmol) in methanol (1.0 mL) was frozen and sealed under vacuum, and placed inside an oven at 110 °C. Pale green platelike crystals were

(17) Compounds **1**−**4** are consistently low in carbon and hydrogen contents, presumably due to surface contamination of the products by insoluble metal carbonates and cupric oxide starting materials.

obtained after 24 h of heating (yield (0.044 g): 85.4%, based on **L**-H_4). Anal. Calcd (found) for [Ni(**L**-H_2)$(MeOH)_4$]: C, 48.9 (46.2); H, 5.57 (4.96). IR (cm^{-1}): 3443 (br), 1622 (s), 1473 (w), 1459 (w), 1343 (w), 1265 (m), 1248 (m), 1143 (s), 1116 (s), 1047 (s), 935 (w), 817 (w), 665 (w), 571 (w).

Synthesis of [Cu(L-Et_2)], 4. In a heavy-walled Pyrex tube a mixture of CuO (0.008 g, 0.1 mmol) and **L**-H_4 (0.050 g, 0.1 mmol) was thoroughly mixed in ethanol (1.0 mL). The tube was frozen, sealed under vacuum, and placed in an oven at 130 °C. After 7 days of heating, 0.038 g of blue-green platelike crystals was obtained (yield: 61.3%, based on **L**-H_4). Anal. Calcd (found) for [Cu(**L**-Et_2)]: C, 54.2 (52.4); H, 4.88 (4.45). IR (cm^{-1}): 2925 (m), 1618 (s), 1466 (s), 1340 (w), 1241 (w), 1112 (s), 1041 (s), 959 (w), 780 (w), 533 (w).

Synthesis of [Zn_3(L-H)$_2$($C_6H_5N)_2$], 5. A heavy-walled Pyrex tube containing a mixture of $Zn(ClO_4)_2 \cdot 6H_2O$ (0.0093 g, 0.025 mmol) and **L**-H_4 (0.0252 g, 0.05 mmol) in methanol (1.0 mL), water (0.1 mL) and pyridine (0.1 mL) was frozen and sealed under vacuum, and placed inside an oven at 110 °C. Colorless platelike crystals were obtained after 24 h of heating (yield (0.0093 g): 82.3%, based on zinc perchlorate). Anal. Calcd (found) for [Zn_3(**L**-H)$_2$($C_6H_5N)_2$]: C, 51.5 (50.8); H, 3.87 (3.69); N, 2.07 (2.14). IR (cm^{-1}): 3075 (w), 2978 (w), 1621 (s), 1530 (w), 1475 (m), 143 8(s), 1343 (m), 1288 (m), 1255 (m), 1247 (w), 1211 (w), 1102 (w), 817 (m), 792 (m), 625 (w), 540 (w).

X-ray Data Collections and Structure Determination. Data collection for **1**−**5** was carried out on a Siemens SMART system equipped with a CCD detector using Mo Kα radiation. All the structures were solved by direct methods[18] and refined on F^2 by full-matrix least squares using anisotropic displacement parameters for all non-hydrogen atoms except those of included solvent molecules. Experimental details for X-ray data collections of **1**−**5** are tabulated in Table 1, while selected bond distances and angles for **1**−**5** are listed in Table S1.

Acknowledgment. We acknowledge NSF (CHE-0208930) for financial support. We also thank Dr. Scott R. Wilson at University of Illinois for X-ray data collection, and Ms. Helen L. Ngo for help with the ligand synthesis. W.L. is an Alfred P. Sloan Fellow, an Arnold and Mabel Beckman Young Investigator, a Cottrell Scholar of Research Corporation, and a Camille Dreyfus Teacher−Scholar.

Supporting Information Available: Experimental procedures, TGA curves, Table S1 (PDF); X-ray crystallographic file (CIF). This material is available free of charge via the Internet at http://pubs.acs.org.

CM0202714

(18) Sheldrick, G. M. *SHELXS-97, Program for Crystal Structure Refinement*; Universität Göttingen: Göttingen, Germany, 1997.